

Performance of Slab Geometry Constraints on Rapid Geodetic Slip Models, Tsunami Amplitude, and Inundation Estimates in Cascadia

Kevin Kwong  * 1,2, Brendan W. Crowell  3, Amy L. Williamson  4, Diego Melgar  5,6, Yong Wei  7,8

¹University of Washington, Department of Earth and Space Sciences, Seattle, Washington, USA, ²California State Polytechnic University, Pomona, Geological Sciences Department, Pomona, CA, USA, ³The Ohio State University, School of Earth Sciences, Columbus, Ohio, USA, ⁴Berkeley Seismology Laboratory, University of California, Berkeley, California, USA, ⁵University of Oregon, Department of Earth Sciences, Eugene, Oregon, USA, ⁶Cascadia Region Earthquake Science Center, Eugene, Oregon, USA, ⁷University of Washington, Cooperative Institute for Climate, Ocean, & Ecosystem Studies, Seattle, Washington, USA, ⁸NOAA/Pacific Marine Environmental Lab, Seattle, WA, USA

Author contributions: *Conceptualization:* Kevin Kwong, Brendan W. Crowell, Diego Melgar. *Data Curation:* Kevin Kwong, Brendan W. Crowell, Amy L. Williamson, Diego Melgar, Yong Wei. *Formal Analysis:* Kevin Kwong, Brendan W. Crowell, Yong Wei. *Funding Acquisition:* Brendan W. Crowell, Diego Melgar. *Investigation:* Kevin Kwong. *Methodology:* Kevin Kwong, Brendan W. Crowell, Amy L. Williamson, Diego Melgar, Yong Wei. *Project Administration:* Kevin Kwong, Brendan W. Crowell, Amy L. Williamson, Diego Melgar, Yong Wei. *Software:* Kevin Kwong, Brendan W. Crowell, Yong Wei. *Supervision:* Brendan W. Crowell, Diego Melgar. *Visualization:* Kevin Kwong, Amy L. Williamson. *Writing – original draft:* Kevin Kwong. *Writing – review & editing:* Kevin Kwong, Brendan W. Crowell, Amy L. Williamson, Diego Melgar, Yong Wei.

Abstract Tsunamigenic megathrust earthquakes along the Cascadia subduction zone present a major hazard concern. We can better prepare to model the earthquake source in a rapid manner by imbuing fault geometry constraints based on prior knowledge and by evaluating the capabilities of using existing GNSS sensors. Near-field GNSS waveforms have shown promise in providing rapid coarse finite-fault model approximations of the earthquake rupture that can improve tsunami modeling and response time. In this study, we explore the performance of GNSS derived finite-fault inversions and tsunami forecasting predictions in Cascadia that highlights the impact and potential of geodetic techniques and data in operational earthquake and tsunami monitoring. We utilized 1300 Cascadia earthquake simulations (*FakeQuakes*) that provide realistic (M7.5-9.3) rupture scenarios to assess how feasibly finite-fault models can be obtained in a rapid earthquake early warning and tsunami response context. A series of fault models with rectangular dislocation patches spanning the Cascadia megathrust area is added to the GFAST inversion algorithm to calculate slip for each earthquake scenario. Another method used to constrain the finite-fault geometry is from the GNSS-derived CMT fault plane solution. For the Cascadia region, we show that fault discretization using two rectangular segments approximating the megathrust portion of the subduction zone leads to improvements in modeling magnitude, fault slip, tsunami amplitude, and inundation. In relation to tsunami forecasting capabilities, we compare coastal amplitude predictions spanning from Vancouver Island (Canada) to Northern California (USA). Generally, the coastal amplitudes derived using fault parameters from the CMT solutions show an overestimation bias compared to amplitudes derived from the fixed slab model. We also see improved prediction values of the run-up height and maximum amplitude at 10 tide gauge stations using the fixed slab model as well.

Production Editor:
Alice Agnes-Gabriel,
Christie Rowe
Handling Editor:
Mathilde Radiguet
Copy & Layout Editor:
Anant Hariharan

Received:
July 7, 2024
Accepted:
January 16, 2025
Published:
February 12, 2025

1 Introduction

Operational tsunami monitoring has traditionally relied on quick earthquake source approximations from seismic data and verification from open ocean buoys and coastal tide gauges that directly measure tsunami waves (e.g., An et al., 2014). However, this reliance on seismic data has limitations; in large earthquakes, the estimate of magnitude in the near-field can saturate, an effect that gets directly propagated into tsunami forecasts (e.g., Hoshiba and Ozaki, 2014). Furthermore, the W-Phase seismic solution (Kanamori, 1993) is often the first reliable magnitude estimate, but rapid results can take up to ~20 minutes or more, relative to the origin time, to obtain (e.g., Hayes et al., 2009). To

aid in a more rapid and proper identification of large earthquakes in the near-field, Blewitt et al. (2006) proposed using Global Navigation Satellite System (GNSS) data. GNSS data is particularly advantageous since it directly measures displacement of the ground in a non-inertial reference frame and does not saturate for the largest earthquakes (Wright et al., 2012; Melgar et al., 2015, 2013). Real-time applications of high-rate GPS data in earthquake early warning (e.g., Allen and Ziv, 2011; Colombelli et al., 2013) have evolved to, in the past decade, include several GNSS-based rapid earthquake source algorithms such as BEFORES (Minson et al., 2014), G-larmS (Grapenthin et al., 2014), REGARD (Kawamoto et al., 2016), and GFAST (Crowell et al., 2016; Murray et al., 2018), the latter recently fully integrated into the U.S. West Coast-wide ShakeAlert system (Murray et al., 2023). ShakeAlert is now the world's first

*Corresponding author: kkwong@uw.edu

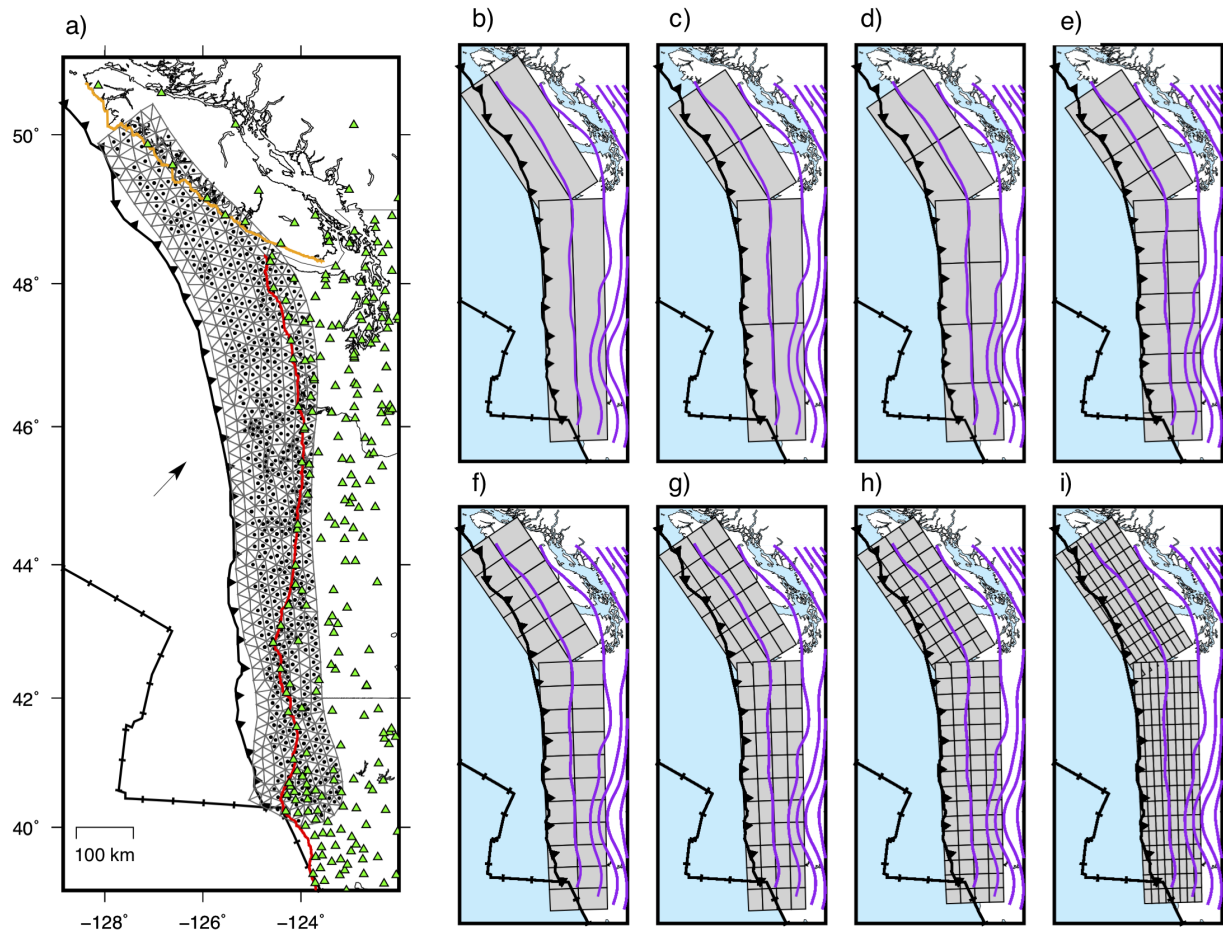


Figure 1 Map view of the Cascadia subduction zone boundary using data from Bird (2003) in the Pacific Northwest. (a) Large left map shows locations of high-rate GNSS stations (green triangles) and epicenter locations of the 1300 events in the *Cascadia FakeQuakes* database (black circles). Triangles with gray outline shown in mapview represent the model mesh for the rupture simulations described in Melgar et al. (2016). The black arrow represents the plate motion of the Juan de Fuca Plate with respect to the North American Plate (GSRM v2.1). Extent of tsunami forecast modeling on the coastline is described by two transects: U.S.A (southern coast), red line and Canada (northern coast), orange line. Smaller maps on the right show discretized fault patch areas (gray rectangles) referred to as Slab models that range in having (b) 4 patches, (c) 8 patches, (d) 12 patches, (e) 24 patches, (f) 34 patches, (g) 68 patches, (h) 100 patches, and (i) 200 patches. Purple contour lines (20 km depth interval) represent depth to the slab interface model from Slab2 (Hayes et al., 2018).

Earthquake Early Warning (EEW) system that utilizes a real-time operating geodetic algorithm.

The GFAST (Geodetic First Approximation of Size and Time) algorithm was initially developed at the University of Washington (UW) to provide rapid characterization of large-magnitude earthquakes by determining estimates of (1) earthquake magnitude from measurements of peak ground displacement (PGD), (2) a centroid moment tensor (CMT) and (3) finite-fault (FF) slip inversion from coseismic offsets. GFAST aims to accurately model GNSS observations to take advantage of the fact that high-rate geodetic displacement data tend to be robust in capturing the true deformation field without the signal going off-scale, consequently alleviating a problematic issue that commonly arises in using traditional seismic data to measure large ground motions (e.g., Melgar et al., 2019; Grapenthin et al., 2017). A major benefit of having GFAST in real-time operation is the improved capability to initially calculate a robust magnitude estimate for a large event.

The debut of GFAST integrating with EEW systems has significant relevance to Tsunami Early Warning (TEW) and tsunami hazard approximation, especially combined with advances in tsunami numerical modeling for quantifying tsunami intensities that involve using rupture models of large subduction zone earthquakes (e.g., Melgar et al., 2016; Crempien et al., 2020). Our study and several others focus on the Cascadia Subduction Zone (CSZ) in the Pacific Northwest (PNW) which has the potential to produce a M9+ earthquake on the megathrust fault and generate a massive tsunami of major consequence at local shorelines (e.g., Satake et al., 2003). New methods in tsunami modeling are appealing for the CSZ region because of the region’s density of onshore GNSS stations. To test the performance of rapid geodetic inversion of earthquake sources, we utilize synthetic rupture scenarios from Melgar et al. (2016) that generated simulated 1-Hz displacement data at the GNSS network locations in Cascadia; these synthetic scenarios are here referred to as *Cascadia FakeQuakes* (Figure 1).

The *Cascadia FakeQuakes* cover the entire Cascadia megathrust seismogenic zone. Modeling realistic rupture scenarios of these events requires knowledge of the fault geometry and, more broadly, the geometry of the regional subducting slab surface. Global models of subduction zone slab geometry divided within major regional slab segments, such as Slab2 (Hayes et al., 2018), updated from Slab1 (Hayes et al., 2012), are available to the public. High-resolution and sophisticated simulations of megathrust earthquake rupture like the *Cascadia FakeQuakes* dataset employ information from slab geometry models that can be used to build complex mesh discretization, for example, triangular mesh elements (e.g., Barnhart and Lohman, 2010) to accurately simulate three-dimensional features of the fault surface (Figure 1a). Currently, inverting GNSS or seismic observations for slip on finely discretized and complex meshes is computationally time-consuming and not immediately applicable to tsunami early warning.

In this study, we examine the role of using predefined fault catalogs in addition to CMT-derived fault geometries to see how these different approaches to fault parameterization impact rapid GNSS source modeling. Williamson et al. (2020) explored GFAST's ability to recreate fault geometries that are comparable with the megathrust using geodetic CMT nodal plane information. They summarized that the finite-fault solutions generally resulted in fault dips steeper ($\sim 30^\circ$) than the expected shallow dipping megathrust geometry ($\sim 9^\circ$) but fault strike solutions were consistent with the rupture simulations. The generation of steeper and deeper GFAST CMT solutions from coseismic offsets arises from the tradeoff between point source and finite source solutions; fitting large offsets over a large geographic area to a single point source requires making the source deeper or rotating the moment tensor. The sources used in that analysis and in the work shown here are predominantly thrust faulting events to evaluate tsunami impact, although we acknowledge that slip on normal "outer-rise" faults, splay faults, and strike-slip faults are useful observations for additional future studies.

We start by exploring various resolutions of fault discretization that will be appropriate to evaluate earthquake source inversions. Here, we construct predefined fault rupture patches along the shallow Cascadia megathrust seismogenic zone and use GFAST to determine finite-fault rupture models using the *Cascadia FakeQuakes* scenarios from Melgar et al. (2016). The 1300 scenarios for the Cascadia subduction zone provide a robust synthetic dataset to test the impact of the chosen fault discretization on the GFAST algorithm results. Specifically, we assess the accuracy of the GNSS-based earthquake and tsunami early warning source products determined within a few minutes after rupture initiation. Improvements in both of these aspects will be useful to implement a modified GFAST monitoring system for Cascadia and may provide additional framework and strategies for constructing and implementing future fault catalogs of other subduction megathrust regions. Finally, we look into run-up and amplitude predictions at tide gauges as another critical component to

validating tsunami forecasting models.

2 Methods

2.1 Overview of Cascadia FakeQuakes

Characterizing variable earthquake and tsunami scenarios is an important strategy for approximating the impact of the hazard. We estimate variable earthquake sources and the resulting tsunami amplitudes using the *FakeQuakes* database showcased in Melgar et al. (2016), which offers an extensive range of stochastically derived rupture scenario data that focus on models of large-magnitude tsunamigenic slip events located across the entire Cascadia megathrust fault region (Figure 1). The *FakeQuakes* are fault-slip models derived from the Karhunen-Loeve (K-L) expansion method (LeVeque et al., 2017) to create synthetic displacement waveform data modeled at the locations of 426 regionally located GNSS stations that encompass networks considered useful to early warning for the Pacific Northwest such as the NOTA, PANGA, and BARD networks.

There are a total of 1300 events in the *FakeQuakes* database, each with a unique stochastic heterogeneous forward slip model (primarily dip-slip solution), moment magnitude (ranging between M7.5 – M9.3) and hypocentral location. The generation of stochastic slip distribution models provides dense and diverse observations for an earthquake-generating fault zone that lacks direct variable observations of historical great earthquakes, such as the 1700 event. A large catalog of rupture scenarios is also useful for probabilistic tsunami hazard assessment, since fault slip can have an important effect on the resulting tsunami. The *FakeQuakes* database provides the opportunity to test the performance of current near-field GNSS configurations and geodetic earthquake and tsunami algorithms for events that occur across the entire Cascadia coastline.

2.2 Slip Model Discretization

For optimizing rapid estimation of slip on a fault, we discretized a fault area with rectangular dislocation subpatches prior to the source inversion process. This approach allows the inversion of multiple segments with varying strike, dip and patch sizes that can better approximate major curvature changes on the subducting megathrust than a single rectangular geometry. We split the Cascadia subduction zone into two main segments; a northern segment striking at $\sim 24^\circ$ NW roughly parallel to the coastline of Vancouver Island (segment 1) and a southern segment stretching from the Mendocino triple junction to the Strait of Juan de Fuca (segment 2), striking $\sim 0^\circ$ NS (Figure 1). Depth to slab surface data from the Slab2 model (Hayes et al., 2018) helped to approximate the geometry of the two segments. We constrain the segment down to a depth of 40 km, the seismogenic depth extent of the *FakeQuakes* dataset. This depth is also roughly the start of the episodic tremor and slip zone in Cascadia (e.g., Nuyen and Schmidt, 2021; Brudzinski and Allen, 2007). These two main fault segments are further subdivided into even rectangular sub-

patches. We showcase 8 different fault model discretizations that range from sub-faults with 25 by 50 km in dimension to 100 by 800 km in size. An overview of the subdivisions is outlined in Table 1 and shown in Figure 1. The fault models with the least and most sub-patches range from 4 and 200 respectively. These predefined fault catalogs will be referenced as the "Slab models".

We tested how "true" slip from the *FakeQuakes* distributed under the rectangular fault sub-patch areas compare in moment release, and how much is recovered. For each of the 1300 stochastic slip distributions, we average the slip on our fault models such that each triangular element (true slip value) beneath a rectangular fault patch was averaged and assigned a moment. The sum of the moment from each patch was used to calculate a separate moment magnitude (M_w) for each event, representative of the moment normalized under a given fault model discretization area. We compared this M_w with the *FakeQuakes* derived M_w to see how our normalized slip models match with the moment from the simulations so there is no magnitude bias in our tsunami predictions (see Supplementary Figure S1).

2.3 Overview of GNSS Slip Modeling

We use the GFAST algorithm (Crowell et al., 2016) to model coseismic slip based on methodologies described in Crowell et al. (2012). Their study showed that regional GPS networks, such as those in western North America and Japan, provide adequate coverage to record the displacements of large earthquakes (e.g. the 2003 M_w 8.3 Tokachi-oki Earthquake and the 2010 M_w 7.2 El Mayor-Cucapah Earthquake). These near-field geodetic data are used to compute finite-fault slip inversions in a homogeneous elastic half-space with Green's functions obtained from Okada (1985). We evaluate the performance of GFAST finite-fault inversions using two different approaches related to fault assumptions but keeping the same physics and modeling setup as previously described. The first approach calculates fault slip assuming no prior knowledge about the fault geometry. In this approach, the preferred geodetic centroid moment tensor (CMT) solution, determined within a separate module in GFAST, and the fault dimensions, calculated from the scaling relations of Blaser et al. (2010), provide the fault model parameters. Thus, the length and width of the slip patch can vary but the number of strike and dip elements is set to 20 and 5 respectively, thus allowing 100 sub-patches. The slip is separately prescribed onto both nodal planes of the CMT solution, and the fault plane with the lowest GNSS residual fit is set as the preferred solution. In the second approach, the fault slip is calculated based on the predefined slab models as described in section 2.2. Slip model solutions for each event are created at specified rupture times at 30 s intervals starting from 30 s to 300 s from the origin time. With both approaches, our regularization constraint requires the rectangular fault patches to be the same size.

2.4 Overview of Tsunami Modeling

The amplitudes of the tsunami waves are predicted using the spatio-temporal information of the coseismic slip. The earthquake slip values are transformed into seafloor deformation by assuming an elastic half-space model (Okada, 1985). This seafloor deformation is instantaneously transformed into sea surface perturbations by assuming an incompressible water column. Two tsunami models are employed to compare tsunami impact offshore and onshore with the "true observations", which are the model results computed from the generic *FakeQuakes*.

We use the GeoClaw software package (Berger et al., 2011) that solves the two-dimensional non-linear shallow-water equations (NSWE) with high-resolution finite-volume methods to perform the tsunami simulation from the input deformation field, which is assisted by the adaptive mesh refinement technique. The code has been benchmarked during the National Tsunami Hazard Mitigation Program (NTHMP) series of benchmark tests (González et al., 2011), and is used in Williamson et al. (2020) with the legacy GFAST results. In the present study, the GeoClaw modeling results are sampled from offshore locations to examine the modeled maximum tsunami amplitudes, not the runup heights onshore, versus the *FakeQuake* "observations". This allows us to inspect large-scale model accuracy along the entire PNW coastline.

The impact of tsunami inundation onshore is calculated using existing tsunami forecast models along the PNW coastlines developed by the NOAA Center for Tsunami Research (NCTR). These forecast models are built upon the Method of Splitting Tsunamis (MOST) model that solves the NSWE in characteristic form with an explicit finite difference scheme. Similar to GeoClaw, MOST is also benchmarked by the NTHMP tests (Synolakis et al., 2009; Lynett et al., 2017) and is the operational model that provides real-time tsunami inundation forecasts at NOAA's Tsunami Warning Centers (TWCs). Each MOST-based forecast model consists of three one-way coupled grids, i.e., model boundary conditions are only passed down in one direction from an outer layer to its inner layer, with increasing grid resolutions. Being an operational tool, a forecast model usually computes tsunami inundation extent and runup heights onshore in the innermost grid with a grid resolution of 2-3 arc sec (~60-90 m). It is worth noting that the MOST-based inundation models compute tsunami waveforms at many National Ocean Service (NOS) tide gauges, including the ones along the PNW coastlines, to provide model validation and evaluation with observations (Tang et al., 2009; Titov et al., 2016; Wei et al., 2008). A Manning's coefficient of 0.025 is used in both models to represent the surface roughness of a bare earth.

3 Results

3.1 Earthquake Magnitude Determination

For the Slab models, the standard deviations of the M_w bias are small (Supplementary Figure S1), and models

No. of Patches	No. of Along Strike	No. of Along Dip	Patch Length (km) Segment 1,2	Patch Width (km) Segment 1,2	Strike (°) Segment 1,2	Dip (°)	% of GFAST best models
4	2	2	450, 800	100, 100	325, 358	11.3	0.4
8	4	2	200, 400	100, 100	325, 358	11.3	7.8
12	6	2	200, 200	100, 100	325, 358	11.3	24.4
24	12	2	200, 100	100, 100	325, 358	11.3	49.4
34	17	2	75, 75	100, 100	325, 358	11.3	59.8
68	17	4	75, 75	50, 50	325, 358	11.3	86.9
100	25	4	50, 50	50, 50	325, 358	11.3	94.5
200	25	8	50, 50	25, 25	325, 358	11.3	99.6

Table 1 Summary of fault parameters for the 8 Slab model discretizations. For each Slab model, we show the percentage of best-fitting GFAST models that selected that model over the fault parameters using the CMT solutions for all the *Cascadia FakeQuake* scenarios.

with a small number of fault patches (4-34) and a large area tend to, on average, overestimate the moment. The moment release from the *Fakequakes* mapped within the areas of our discrete fault models shows a small magnitude bias, so we feel confident in using the eight models to resolve magnitude and slip. We compare GFAST’s magnitude estimates with results calculated using the eight predefined slab models and the CMT method. To estimate the magnitude residuals (the difference between the calculated and true magnitude) corresponding to the 1300 events, the GFAST determined magnitudes are subtracted from the “true” M_w from the rupture scenario. While our approach computes a source model that includes a magnitude estimate at 30 s intervals from the origin time to 300 s after, we emphasize that analysis of robust results in under 3 minutes (180 s) is a goal we hope to achieve in geodetic tsunami early warning, as it would show an improvement in the speed of rapid response compared to traditional seismic methods. Figure 2 shows the statistical distribution of the magnitude residuals at 60 s, 120 s and 180 s after the earthquake source origin time. The median residual is within -0.5 to 0.5 for both the CMT and slab model derived model results. We observe a systematic trend; the median magnitude residual increases with increasing number of sub-faults over the total fault area. We attribute this systematic trend in magnitude to the generalized regularization equation proposed in [Crowell et al. \(2012\)](#) that was optimized for fewer fault patches; the use of a generalized regularization equation reduces computation time significantly since the inversion does not need to search for the optimal smoothness (i.e., L-curve norm tradeoff). Another trend is that the spread in the magnitude residual decreases with increase in source duration time. We also see that the Variance Reduction (VR) decreases significantly for the predefined slab model results as the number of sub-patches increases. The VR spread becomes tighter and smaller compared to the CMT results for the Slab models with 34 to 200 patches.

3.2 GFAST Rupture Models

With eight slab model discretizations, we analyze which models can resolve heterogeneous slip and provide better fit to the data compared to the models using the CMT parameters. We specifically explore whether coarse finite-fault models provide a meaningful interpretation of the rupture. The Slab models share the same fault location, geometry, and roughly span the same area as the shallow Cascadia segment from the Slab2 model (Figure 1). In contrast, the event’s unique fault parameters from the CMT solution provide varying fault locations on a single rectangular plane and the geometry is derived from the nodal plane solutions of the moment tensor. To fix outlier geometry models, the input of a known slab model will ensure an accurate fault location for modeling slip on the megathrust. Our results will focus on the spatial and temporal pattern of the finite-fault models determined in under three minutes and differences in modeling slip using a two segment fault model that approximate the known slab location.

The highly discretized Slab models tend to provide better fits to the data (Table 1). The GFAST algorithm chooses between three models with the lowest RMS to the GNSS data; either of the two nodal planes from the CMT inversion or from the specified slab model. Results using the *Cascadia Fakequakes* dataset show our most simplistic fault discretization (4 rectangular patches) is only chosen 0.4% of the time while the rest of the 1300 event database prefers the CMT derived solution. Further model discretization increases the likelihood that it will be the chosen fault model. For instance, the 24 sub-patch model is chosen 49% of the time and the 100 sub-patch model is chosen 94% of the time. These statistics are indicated under “% of GFAST best models” in Table 1.

An important case for using GNSS technology is whether near-field geodetic inversions of high-rate displacement data can recover slip patterns that resemble the earthquake rupture. We highlight three specific rupture scenarios (Earthquake A, B, and C) that illustrate heterogeneous slip variability across the Cascadia megathrust (Figure 3a,b,c). Earthquake A (M8.73) ini-

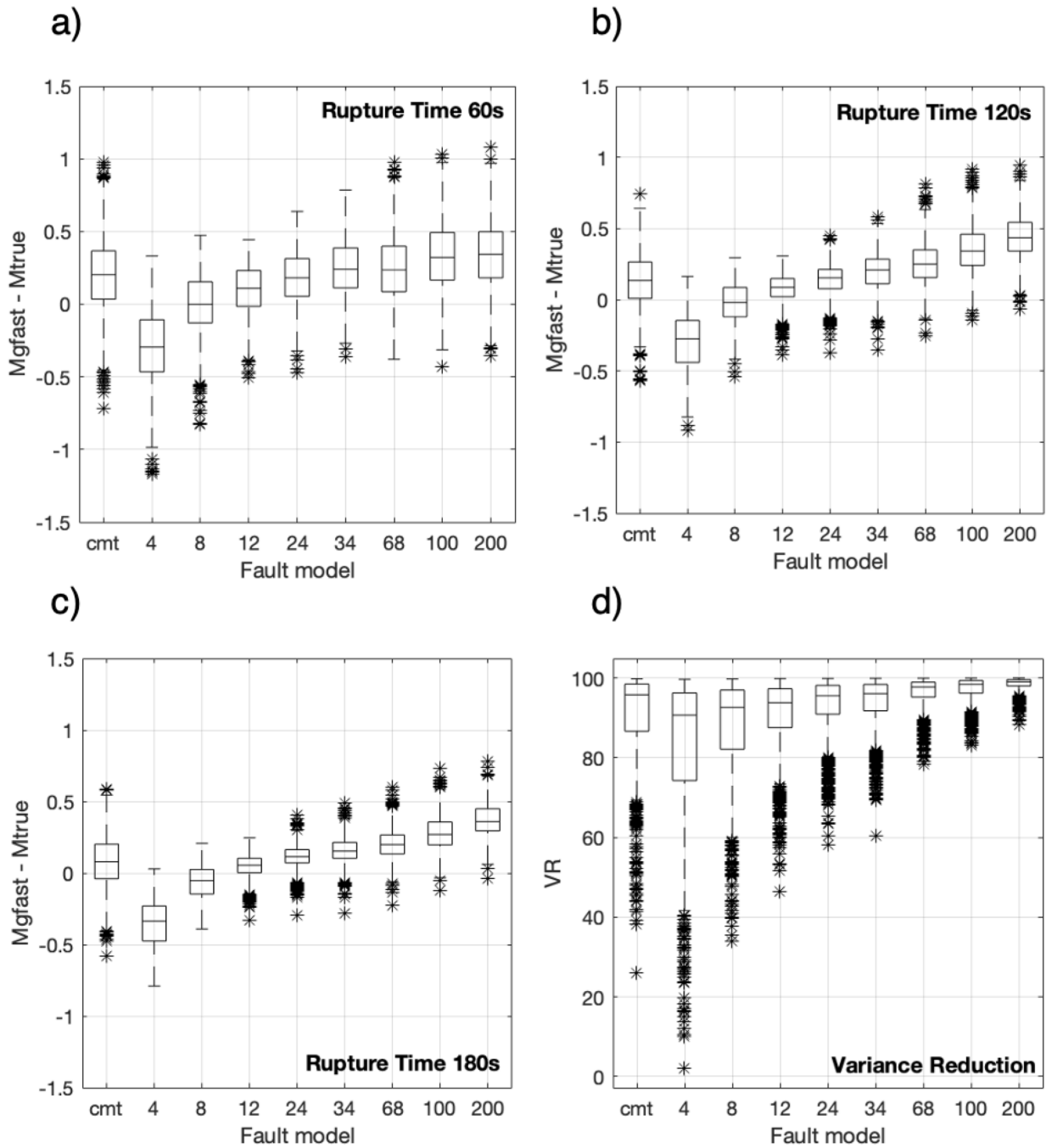


Figure 2 Magnitude residuals (between GFAST and *Cascadia Fakequakes* “true” magnitude) using 8 different pre-defined fault catalogs (Fault model number indicates number of fault sub-patches) and the best fit CMT nodal plane for rupture time at (a) 60 (b) 120 and (c) 180 seconds. (d) Variance reduction at 180 seconds for the same group of fault models. The horizontal line inside the box indicates the median value and the box extends to the 25th percentile (bottom edge) and to the 95th percentile (top edge). Star-shaped symbols indicate outlier points outside the minimum and maximum variability (whisker line) from the upper and lower quartiles.

tiates off the coast of Vancouver Island and Washington State and ruptures to the south, with a large slip asperity located off the northern coast of Oregon. The mostly-unilateral slip distribution is ~300 km in length, with a maximum slip of ~25 km. Earthquake B (M9.08) initiates where the megathrust is changing from a NNW to a roughly NS strike fault. The slip distribution is located updip with a rupture length of ~600-700 km. Earthquake C (M9.01) features a ~500 km length bilateral rup-

ture pattern in the southern portion of the fault. These scenarios represent diverse rupture patterns along various parts of the Cascadia megathrust.

The resulting finite-fault model solutions we highlight here come from the fixed slab and CMT-geometry models, both containing 100 rupture patches. Figure 3d,e shows GFAST finite-fault results of Earthquake A using the slab model and CMT model parameters. Both models show a compact unilateral rupture pattern. The

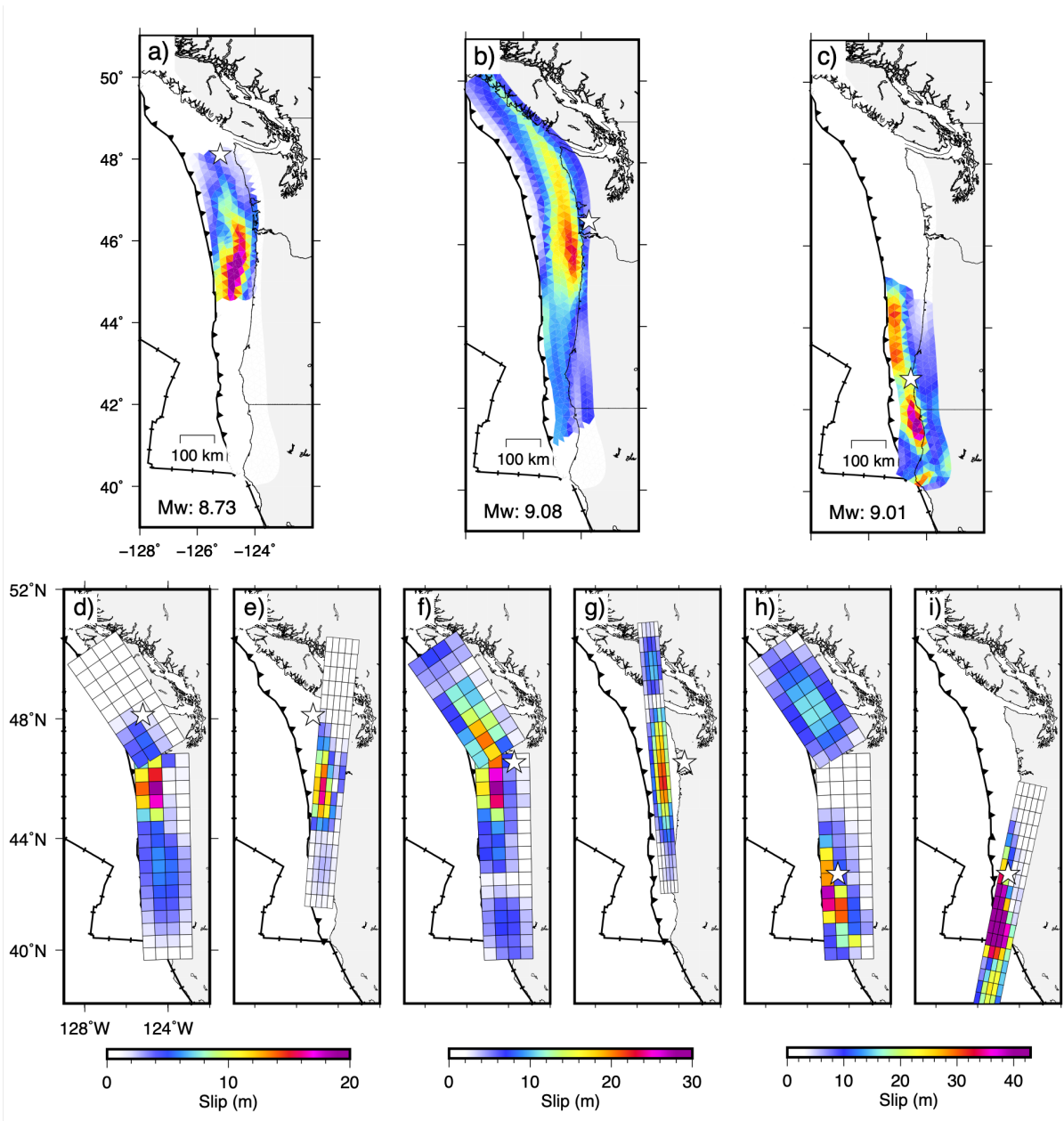


Figure 3 Cascadia Fakequakes rupture scenarios for a) Earthquake A, b) Earthquake B, and c) Earthquake C. GFAST finite-fault model results at 180 s from origin time with two types of fault location and geometry constraints (slab model and CMT) for Earthquake A, d) slab model e) CMT, Earthquake B, f) slab model, g) CMT, Earthquake C, h) slab model, i) CMT. The three fault slip scale bars from left to right correspond uniquely to Earthquake A, B and C. White star indicates earthquake epicenter location.

CMT strike of the fault is 43° NE, which directs the fault away from the Vancouver Island coastline. Despite the two finite-fault models having different strikes, they both capture the main slip in roughly the same location. The simulation of Earthquake B illustrates an almost full rupture of the Cascadia megathrust. The GFAST finite-fault slab model shows high-slip (15-30 m) directly updip from the epicenter at the edges of the two adjoining fault segments and captures slip on both segments along the coastline (Figure 3f). The CMT-based solution shows a 138° striking fault and a concentrated high-slip region updip from the epicenter but the fault extends directly into East Vancouver Island and bypasses the coastline to the north (Figure 3g). The slab model is more reliable in resolving a long rupture where a signif-

icant change in strike in the subduction zone is present. Earthquake C is similar in moment release to Earthquake B but has a more compact slip distribution located off-shore southern Cascadia. The CMT-based solution places a higher concentration of slip south of the epicenter compared to the slab model (Figure 3h,i). Superfluous slip in the slab model (Figure 3h) is located in the northern fault segment, an area that did not rupture in the Earthquake C simulation. The geometry of the CMT solution does not align well with the megathrust location and the high slip region is placed seaward from the trench.

3.3 GFAST Tsunami Amplitude Predictions

We compare tsunami predictions based on the *Cascadia Fakequakes* scenarios (observations) and GFAST finite-fault solutions (models). In Figure 4, the composite dataset indicates deviations in tsunami amplitude predictions with respect to magnitude. The increasing variation in amplitude predictions with increasing magnitude reflects the larger extent of tsunami impact along the coast, associated with complex and larger magnitude ruptures. The median amplitude bias (observations - model) are within -0.8 to 0 m for events with $M > 7$ and $M < 9$. Events with $M > 9$ show the most noticeable difference in amplitude bias between the two model datasets (CMT vs slab model). The median amplitude bias using the CMT fault and slab model is -2.2 and -0.5 m respectively. The negative values reflect a tendency of amplitude overestimation relative to observations. Analyses of the 1300 events help provide statistical descriptions of how the amplitude bias is more significant when using the CMT solutions in comparison to the slab model.

To illustrate the range of tsunami variation along the coast, we highlight three cases. Earthquakes A, B and C from Figure 3 are translated into coastal tsunami amplitudes referred to as Tsunami A, B and C (Figure 5 and 6). The tsunami amplitudes (at 0.25° latitude and longitude intervals) were computed along two coastal transects, one along Vancouver Island, British Columbia and one along the northwestern United States. The observed tsunami is compared to the tsunami based on the slab model (Figure 5) and CMT parameters (Figure 6). We show results at 3 minutes after the origin time to highlight the performance of advance warning at this temporal limit. The peak coastal amplitude for Tsunami A is ~ 12 m at 45° latitude, the slab model's prediction at this location is ~ 7 m, and the CMT parameter model predicts an amplitude of ~ 9 m.

In Tsunami B, the modeled coastal amplitudes (up to 22 m) exceed the observations (~ 9 m) in the southern region. However, the slab model does not overpredict the observations as much as the model from the CMT geometry. In Tsunami C, the models underpredict the maximum amplitude area and overpredict amplitudes at locations specifically along the Vancouver Island coastline. The CMT-geometry based model overpredicts the tsunami amplitudes specifically at regions with latitudes between 39° to 43° , with peak amplitudes at ~ 60 m. Predictions from the slab model are below 25 m and are closer to the observations.

3.4 Inundation Modeling

The main assessment of the MOST-based inundation modeling study is to compare the GFAST finite-fault (CMT vs. Slab model) results to the *Cascadia Fakequakes* measurements. For the present study, we modeled the tsunami impact resulting from the GFAST finite-fault models for 10 coastal communities along the coast: Port Angeles, Neah Bay, La Push, Westport in Washington, Garibaldi, Newport, Florence, Port Orford in Oregon, and Crescent City and Eureka in California. It is worth noting that there is currently no tide gauge that is being

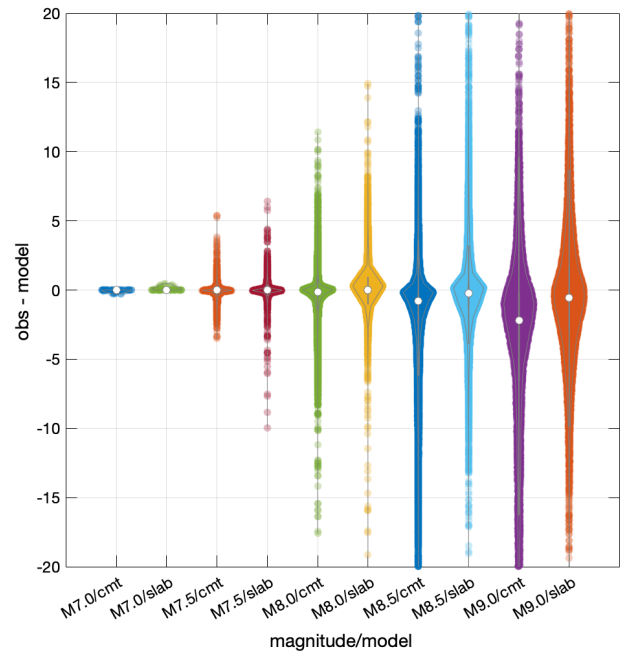


Figure 4 Statistical representation of tsunami amplitude residual (in meters) from all 1300 scenario events between the observations (*Cascadia Fakequakes*) and predictions (GFAST models) with respect to earthquake magnitude and fault model type. For each box plot, the data distribution is sorted in 0.5 magnitude bins with respect to either the CMT or slab model, and the white circle inside the density distribution represents the median value.

operated in Florence, Oregon to provide real-time water level observation. Instead, we placed a virtual gauge at Florence, also termed as a “warning point”, that can provide rapid model estimates of wave amplitudes at the shore during an event. Overall, comparisons of runup height and maximum amplitude at the tide gauge show that, statistically, the Slab model predictions are more accurate to the *FakeQuakes* than the CMT geometry predictions.

Figure 7 summarizes the model accuracies of runup heights and the maximum tsunami amplitude at tide gauge locations at the 10 sites and also features the average values combined from those sites. The model accuracy is calculated as the ratio between the model results and the *FakeQuake* “observations”. One can observe a significant improvement in model accuracy when using the GFAST Slab model over the GFAST CMT model. The improvements in runup height estimate range from 26.0% (Eureka) - 72.5% (Garibaldi), with an average of 45.7% improvement across all 10 sites, reducing the average error from 167.69% using GFAST CMT models to 121.99% using GFAST Slab models. Similar improvements in accuracy can be also seen from the maximum tsunami amplitude estimate at the tide gauge locations, with the average reduced from 182.94% (GFAST CMT) to only 130.93% (GFAST Slab), a 51.9% improvement in model accuracy. The GFAST Slab model is able to reduce the model errors to $\sim 20\%$ for runup heights and $\sim 30\%$ for tide gauge observations, which fit well within the goal of achieving model accuracy greater than 70%

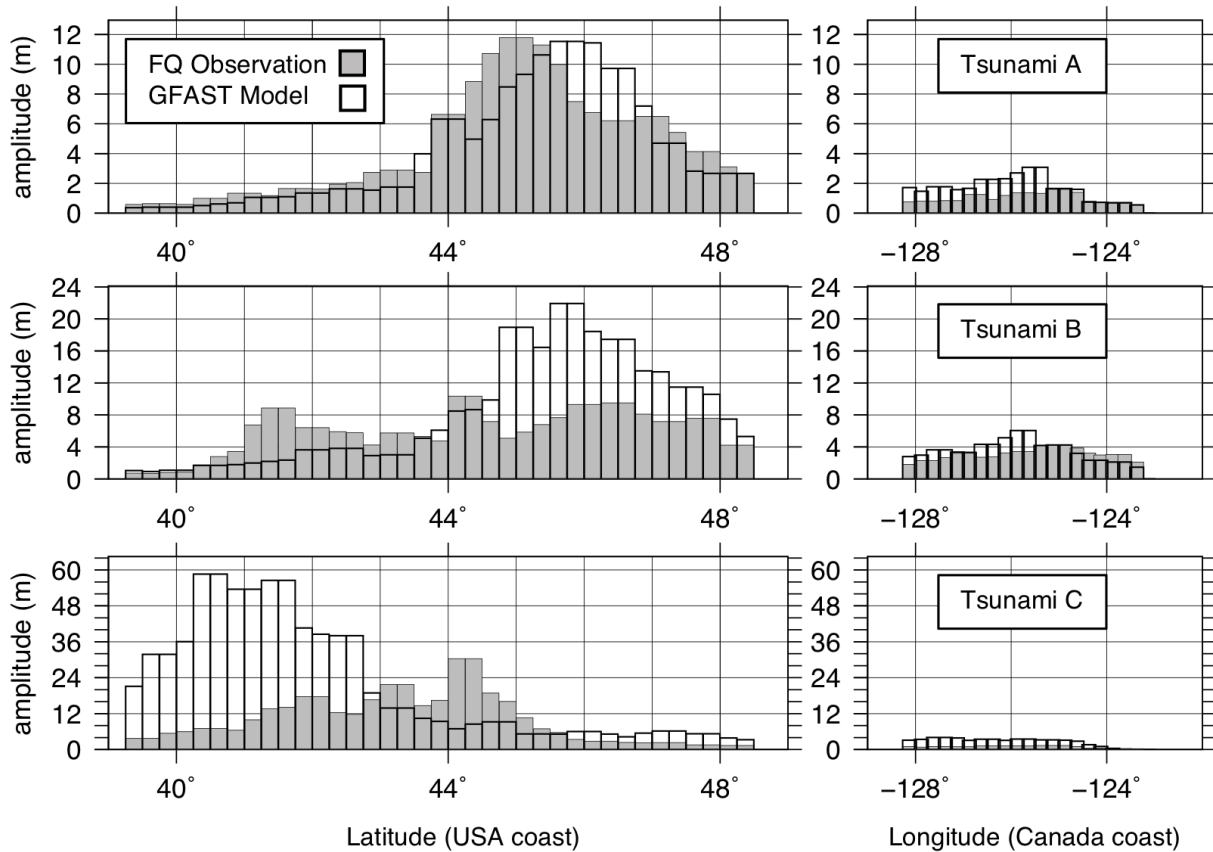


Figure 5 Observed (gray-filled bar) and modeled (hollow bar) maximum tsunami amplitude (m) along the coastline in 0.25° bins along latitude (southern coast) and longitude (northern coast). Refer to map in Figure 1 of the coastline transect locations for the tsunami forecasting. Tsunami A, B and C were modeled from Earthquake A, B and C respectively. The GeoClaw-modeled tsunami amplitude is derived from the GFAST finite-fault model using the CMT parameters.

for tsunami model forecast at the TWCs. Furthermore, at four tide gauge locations (Neah Bay, Westport, Newport, and Florence), the GFAST Slab models are capable of providing spot-on, 98-100%, predictions of the Fake-Quake observations. It is also worth noting that with impressive increases of the model accuracies, the GFAST Slab model gives conservative model forecast results for nine out of ten of the coastal communities, except for the ~5% underestimation of the runup heights at Newport. Importantly, we document the performance of the two different finite-fault modeling approaches for varying fault geometries to highlight the variability in inundation modeling results.

4 Discussion

GFAST offers a complementary toolset to obtain tsunami forecasts from earthquake source products and has the potential to be used concurrently with existing tsunami warning operations that use seismic measurements to rapidly determine an earthquake's size and use deep-water pressure sensors to track the propagation of tsunami waves. Through this study, we highlight the use of technology such as GFAST to enhance the real-time tsunami warning infrastructure in the Pacific Northwest in the context of measuring and

modeling a scenario like a magnitude 9+ earthquake and tsunami. The last megathrust event occurred in 1700 and tsunami deposits indicate an average recurrence interval of 500-600 years (e.g., Peters et al., 2007) which may suggest that Cascadia is late in the interseismic cycle. Observationally, near-field GNSS stations in the PNW have not recorded a significant enough event (M6.5+) within its region outside of the Mendocino fracture zone.

We find improvements in magnitude estimation, data variance reduction, and tsunami wave height and inundation estimation, when adding a fixed fault catalog to GFAST and moreover, find better performance when including more fault patches, allowing for greater slip heterogeneity. We plan to add to GFAST the option to compute rapid geodetic source models using pre-defined global fault databases that contain location points representing a 3D mesh model of the fault. The fault databases address the difficulties in constraining fault parameters using rapid inversion techniques and operations. Williamson et al. (2020) showed that modeling large ruptures on a subduction zone using a single, planar fault model can lead to improbable fault parameters. Fault geometries derived from independent CMT solutions can result in models with locations and geometry that are not consistent with published slab geome-

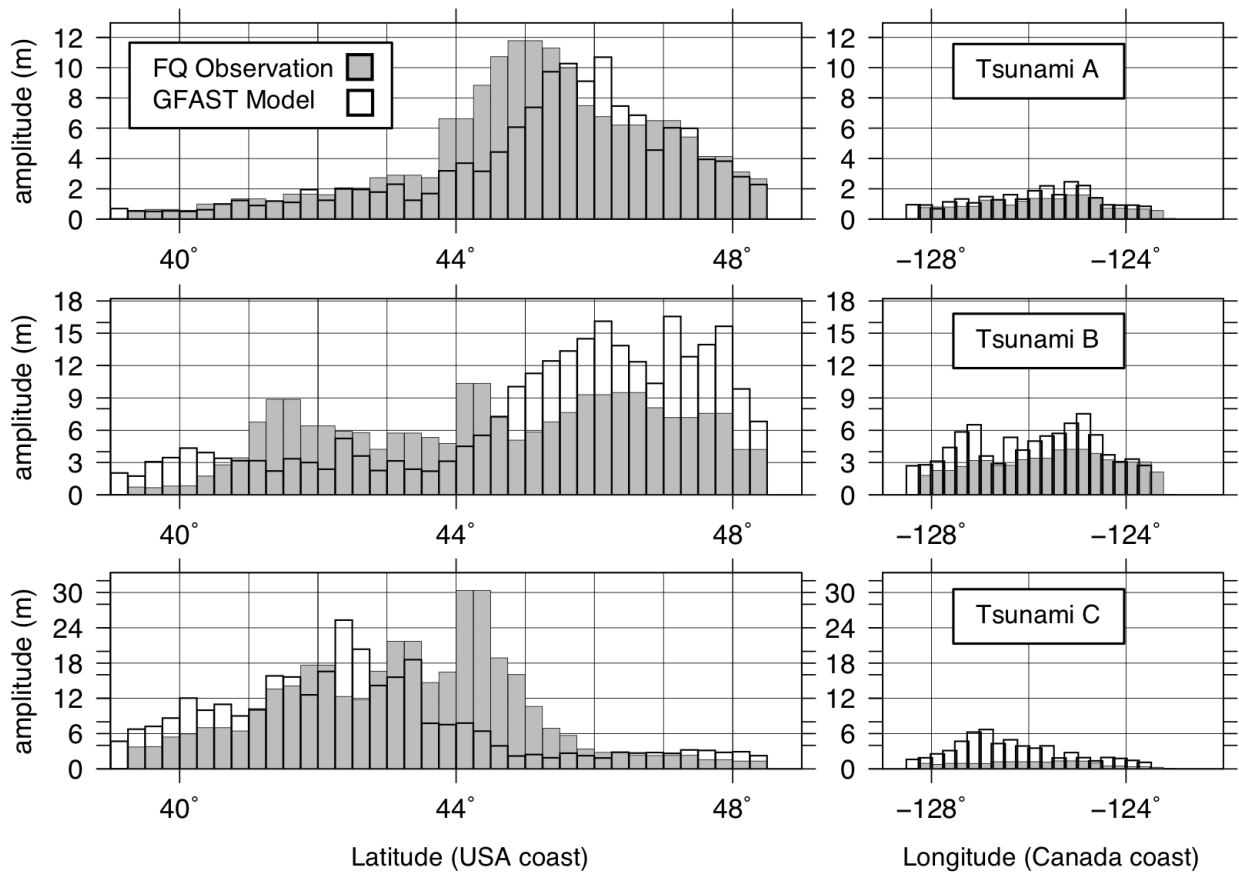


Figure 6 Same description as Figure 5, but the GeoClaw-modeled tsunami amplitude is derived from the GFAST finite-fault model using the Slab model (100 patches).

try models (e.g. Slab2). Fault mesh models that realistically describe the active tectonic region are used to improve the characterization of large complicated earthquake ruptures. Earthquakes with full and long ruptures on non-planar faults are not efficiently described with a single rectangular fault solution. Using the CMT parameters for a single fault plane in GFAST has resulted in difficulty in constraining ruptures along notable fault curvature regions such as the Cascadia slab. The east-ward convex bend along the Cascadia slab is located between the transition from Washington to Vancouver Island and Southwestern British Columbia (Figure 1). The global database of 3D subduction zone geometry (Slab2), helped guide the reconstruction of a simplified fault discretization model for Cascadia. The fault mesh still preserves a rectangular planar geometry but hosts two fault segments that accommodate major along-strike variations of the fault. Nonetheless, retaining the option for the CMT-based slip inversions will allow GFAST to respond to complex ruptures, blind thrusts, splay faults, and other sources with geometries that are not well known prior to the event.

The discretized 100-patch slab model is highlighted in this study to assess the performance with regional GNSS data to determine earthquake magnitude and fault-slip for the Cascadia subduction zone. Rapid estimates of the earthquake size that can overcome magnitude saturation effects under 3 minutes using GNSS stations bring a more modern approach to minimizing the delay time

of forecasts at the TWCs. The comparison of GFAST derived M_w to the true magnitudes of the synthetic events in this study indicates the potential for integrating moment magnitudes from GNSS data for NOAA's Tsunami warning system operations. Automating GNSS finite-fault models is a more complicated but useful methodology in translating the earthquake source to the tsunami hazard domain, using information about fault slip to calculate tsunami amplitudes at the coastline. The slab discretization model with 100 rectangular patches is an appropriate fault catalog to use to model Cascadia subduction zone megathrust events. Example scenarios shown in the study highlight the ability of GFAST finite-fault inversions to resolve discrete slip asperities defined by 100 fault patches across the shallow Cascadia slab region and to recreate heterogenous slip distributions that roughly resemble the synthetic models. The prescribed sub-patch size (50 x 50 km) provides adequate spatial slip variability. While GFAST is fairly computationally efficient, incorporating a finer fault grid with more fault patches would potentially cause the inversion to fall behind real-time timescales (i.e., each iteration takes longer than 1 second), and thus, we find the 100 fault patch model to be sufficiently detailed without sacrificing real-time performance.

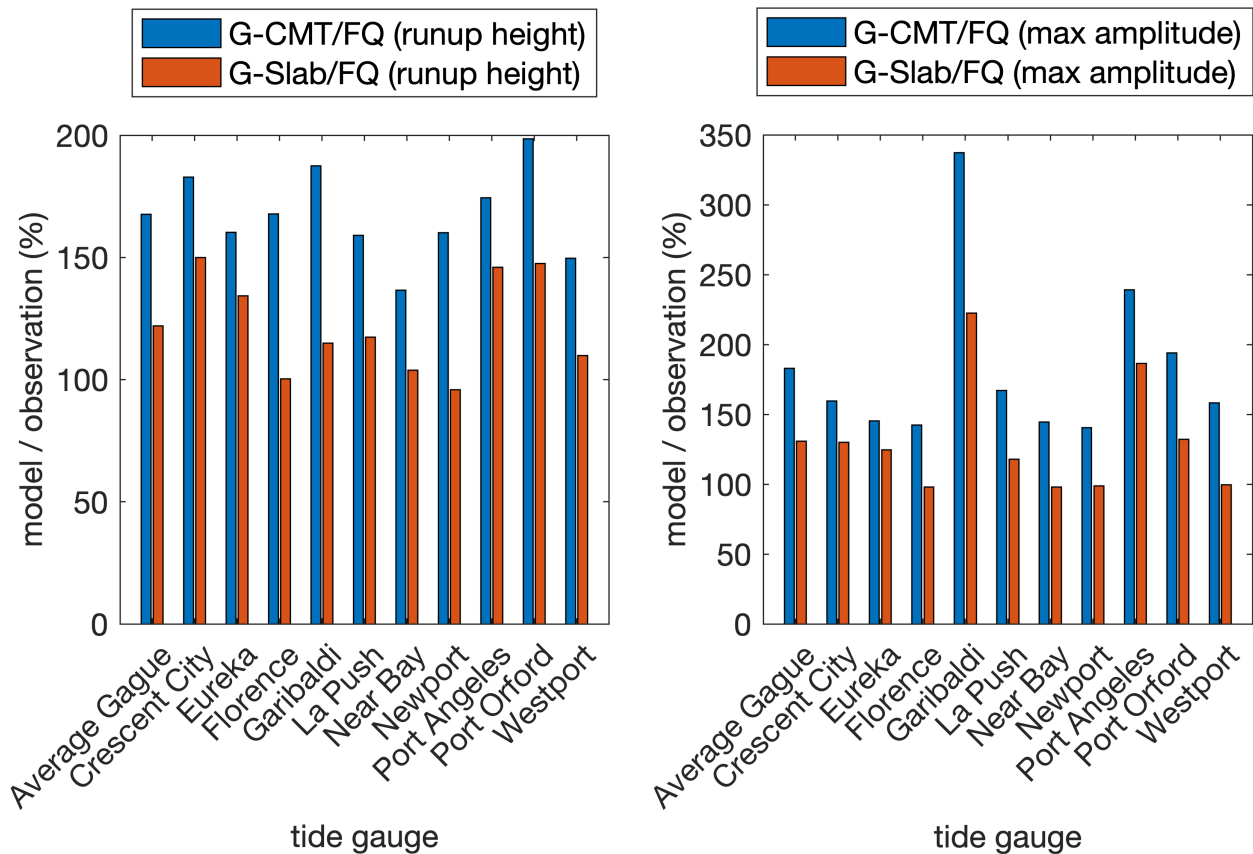


Figure 7 Summary of Model Accuracy of Runup Heights and Max Tsunami Amplitude at Tide Gauge Locations for 10 Coastal Communities along the PNW Coasts. G-CMT = model results obtained from GFAST CMT models; G-Slab = model results obtained from GFAST Slab models; FQ = “observations” obtained from the *FakeQuakes*.

5 Conclusion

Adding catalogs of known faults is a worthwhile priority to incorporate into GFAST inversion strategies. As shown in this study, a discretized slab model that contains reliable fault geometry information improves inversions for early finite-fault rupture models and resolves the issue of finite-fault models positioned in inaccurate locations. The finite-fault models provide detailed slip information that is useful to infer local coastal tsunami amplitude information. We show that GFAST inversions using the slab model tend to result in a lower model RMS and also result in more accurate coastal tsunami amplitude estimates compared to using the CMT solution as the fault geometry constraint.

Local real-time GNSS data is a technology that is proving to enhance rapid earthquake and tsunami monitoring in several regions around the world. Tsunami hazards along the Cascadia coastline are better assessed with detailed rupture simulations that illustrate the variability of tsunami-generating earthquakes. Going forward to other subduction zones and tsunami generating regions, generation of predefined fault catalogs is an impactful goal for tsunami early warning.

Acknowledgements

This work is funded under the NASA Disasters program, grant number 80NSSC19K1104 P00001 to the University

of Oregon and the University of Washington. We would like to thank the reviewers for their time and insightful feedback.

Data and code availability

For earthquake modeling, the GFAST module is available at the Pacific Northwest Seismic Network GitHub repository (<https://github.com/pnsn/GFAST>). For tsunami modeling, the GeoClaw module is available at <https://www.clawpack.org/geoclaw.html>. Files to the earthquake and tsunami models are available in our Zenodo repository (<https://zenodo.org/records/12746085>).

Competing interests

The authors declare no competing interests.

References

- Allen, R. M. and Ziv, A. Application of real-time GPS to earthquake early warning. *Geophysical Research Letters*, 38(16), 2011. doi: <https://doi.org/10.1029/2011GL047947>.
- An, C., Sepúlveda, I., and Liu, P. L.-F. Tsunami source and its validation of the 2014 Iquique, Chile, earthquake. *Geophysical Research Letters*, 41(11):3988–3994, 2014. doi: <https://doi.org/10.1002/2014GL060567>.
- Barnhart, W. D. and Lohman, R. B. Automated fault model discretization for inversions for coseismic slip distributions. *Jour-*

- Journal of Geophysical Research: Solid Earth*, 115(B10), 2010. doi: <https://doi.org/10.1029/2010JB007545>.
- Berger, M. J., George, D. L., LeVeque, R. J., and Mandli, K. T. The GeoClaw software for depth-averaged flows with adaptive refinement. *Advances in Water Resources*, 34(9):1195–1206, 2011. doi: <https://doi.org/10.1016/j.advwatres.2011.02.016>.
- Bird, P. An updated digital model of plate boundaries. *Geochemistry, Geophysics, Geosystems*, 4(3), 2003. doi: <https://doi.org/10.1029/2001GC000252>.
- Blaser, L., Krüger, F., Ohrnberger, M., and Scherbaum, F. Scaling Relations of Earthquake Source Parameter Estimates with Special Focus on Subduction Environment. *Bulletin of the Seismological Society of America*, 100(6):2914–2926, 12 2010. doi: [10.1785/0120100111](https://doi.org/10.1785/0120100111).
- Blewitt, G., Kreemer, C., Hammond, W. C., Plag, H.-P., Stein, S., and Okal, E. Rapid determination of earthquake magnitude using GPS for tsunami warning systems. *Geophysical Research Letters*, 33(11), 2006. doi: <https://doi.org/10.1029/2006GL026145>.
- Brudzinski, M. R. and Allen, R. M. Segmentation in episodic tremor and slip all along Cascadia. *Geology*, 35(10):907–910, 10 2007. doi: [10.1130/G23740A.1](https://doi.org/10.1130/G23740A.1).
- Colombelli, S., Allen, R. M., and Zollo, A. Application of real-time GPS to earthquake early warning in subduction and strike-slip environments. *Journal of Geophysical Research: Solid Earth*, 118(7):3448–3461, 2013. doi: <https://doi.org/10.1002/jgrb.50242>.
- Crempien, J. G., Urrutia, A., Benavente, R., and Cienfuegos, R. Effects of earthquake spatial slip correlation on variability of tsunami potential energy and intensities. *Scientific reports*, 10(1):8399, 2020. doi: <https://doi.org/10.1038/s41598-020-65412-3>.
- Crowell, B. W., Bock, Y., and Melgar, D. Real-time inversion of GPS data for finite fault modeling and rapid hazard assessment. *Geophysical Research Letters*, 39(9), 2012. doi: <https://doi.org/10.1029/2012GL051318>.
- Crowell, B. W., Schmidt, D. A., Bodin, P., Vidale, J. E., Gomberg, J., Renate Hartog, J., Kress, V. C., Melbourne, T. I., Santillan, M., Minson, S. E., et al. Demonstration of the Cascadia G-FAST geodetic earthquake early warning system for the Nisqually, Washington, earthquake. *Seismological Research Letters*, 87(4): 930–943, 2016. doi: <https://doi.org/10.1785/0220150255>.
- González, F., LeVeque, R., Varkovitzky, J., Chamberlain, P., Hirai, B., and George, D. GeoClaw results for the NTHMP tsunami benchmark problems. In *Results of the 2011 NTHMP Model Benchmarking Workshop*, 2011.
- Grapenthin, R., Johanson, I. A., and Allen, R. M. Operational real-time GPS-enhanced earthquake early warning. *Journal of Geophysical Research: Solid Earth*, 119(10):7944–7965, 2014. doi: <https://doi.org/10.1002/2014JB011400>.
- Grapenthin, R., West, M., and Freymueller, J. The Utility of GNSS for Earthquake Early Warning in Regions with Sparse Seismic Networks. *Bulletin of the Seismological Society of America*, 107(4): 1883–1890, 06 2017. doi: [10.1785/0120160317](https://doi.org/10.1785/0120160317).
- Hayes, G. P., Rivera, L., and Kanamori, H. Source Inversion of the W-Phase: Real-time Implementation and Extension to Low Magnitudes. *Seismological Research Letters*, 80(5):817–822, 09 2009. doi: [10.1785/gssrl.80.5.817](https://doi.org/10.1785/gssrl.80.5.817).
- Hayes, G. P., Wald, D. J., and Johnson, R. L. Slab1.0: A three-dimensional model of global subduction zone geometries. *Journal of Geophysical Research: Solid Earth*, 117(B1), 2012. doi: <https://doi.org/10.1029/2011JB008524>.
- Hayes, G. P., Moore, G. L., Portner, D. E., Hearne, M., Flamme, H., Furtney, M., and Smoczyk, G. M. Slab2, a comprehensive subduction zone geometry model. *Science*, 362(6410):58–61, 2018. doi: [10.1126/science.aat4723](https://doi.org/10.1126/science.aat4723).
- Hoshiba, M. and Ozaki, T. *Earthquake Early Warning and Tsunami Warning of the Japan Meteorological Agency, and Their Performance in the 2011 off the Pacific Coast of Tohoku Earthquake (Mw 9.0)*, pages 1–28. Springer Berlin Heidelberg, Berlin, Heidelberg, 2014. doi: [10.1007/978-3-642-12233-0_1](https://doi.org/10.1007/978-3-642-12233-0_1).
- Kanamori, H. W phase. *Geophysical Research Letters*, 20(16): 1691–1694, 1993. doi: <https://doi.org/10.1029/93GL01883>.
- Kawamoto, S., Hiyama, Y., Ohta, Y., and Nishimura, T. First result from the GEONET real-time analysis system (REGARD): the case of the 2016 Kumamoto earthquakes. *Earth, Planets and Space*, 68:1–12, 2016. doi: <https://doi.org/10.1186/s40623-016-0564-4>.
- LeVeque, R. J., Waagan, K., González, F. I., Rim, D., and Lin, G. *Generating Random Earthquake Events for Probabilistic Tsunami Hazard Assessment*, pages 3671–3692. Springer International Publishing, Cham, 2017. doi: [10.1007/978-3-319-55480-8_2](https://doi.org/10.1007/978-3-319-55480-8_2).
- Lynett, P. J., Gately, K., Wilson, R., Montoya, L., Arcas, D., Aytore, B., Bai, Y., Bricker, J. D., Castro, M. J., Cheung, K. F., David, C. G., Dogan, G. G., Escalante, C., González-Vida, J. M., Grilli, S. T., Heitmann, T. W., Horrillo, J., Kânoğlu, U., Kian, R., Kirby, J. T., Li, W., Macías, J., Nicolsky, D. J., Ortega, S., Pampell-Manis, A., Park, Y. S., Roeber, V., Sharghivand, N., Shelby, M., Shi, F., Tehranirad, B., Tolkova, E., Thio, H. K., Velioglu, D., Yalçiner, A. C., Yamazaki, Y., Zaytsev, A., and Zhang, Y. Inter-model analysis of tsunami-induced coastal currents. *Ocean Modelling*, 114:14–32, 2017. doi: <https://doi.org/10.1016/j.ocemod.2017.04.003>.
- Melgar, D., Crowell, B. W., Bock, Y., and Haase, J. S. Rapid modeling of the 2011 Mw 9.0 Tohoku-oki earthquake with seismogeodesy. *Geophysical Research Letters*, 40(12):2963–2968, 2013. doi: <https://doi.org/10.1002/grl.50590>.
- Melgar, D., Crowell, B. W., Geng, J., Allen, R. M., Bock, Y., Riquelme, S., Hill, E. M., Protti, M., and Ganas, A. Earthquake magnitude calculation without saturation from the scaling of peak ground displacement. *Geophysical Research Letters*, 42(13):5197–5205, 2015. doi: <https://doi.org/10.1002/2015GL064278>.
- Melgar, D., LeVeque, R. J., Dreger, D. S., and Allen, R. M. Kinematic rupture scenarios and synthetic displacement data: An example application to the Cascadia subduction zone. *Journal of Geophysical Research: Solid Earth*, 121(9):6658–6674, 2016. doi: <https://doi.org/10.1002/2016JB013314>.
- Melgar, D., Melbourne, T. I., Crowell, B. W., Geng, J., Szeliga, W., Scrivner, C., Santillan, M., and Goldberg, D. E. Real-Time High-Rate GNSS Displacements: Performance Demonstration during the 2019 Ridgecrest, California, Earthquakes. *Seismological Research Letters*, 91(4):1943–1951, 12 2019. doi: [10.1785/0220190223](https://doi.org/10.1785/0220190223).
- Minson, S. E., Murray, J. R., Langbein, J. O., and Gomberg, J. S. Real-time inversions for finite fault slip models and rupture geometry based on high-rate GPS data. *Journal of Geophysical Research: Solid Earth*, 119(4):3201–3231, 2014. doi: <https://doi.org/10.1002/2013JB010622>.
- Murray, J. R., Crowell, B. W., Grapenthin, R., Hodgkinson, K., Langbein, J. O., Melbourne, T., Melgar, D., Minson, S. E., and Schmidt, D. A. Development of a geodetic component for the US West Coast earthquake early warning system. *Seismological Research Letters*, 89(6):2322–2336, 2018. doi: <https://doi.org/10.1785/0220180162>.
- Murray, J. R., Crowell, B. W., Murray, M. H., Ulberg, C. W., McGuire, J. J., Aranha, M. A., and Hagerty, M. T. Incorporation of Real-Time Earthquake Magnitudes Estimated via Peak Ground Displacement Scaling in the ShakeAlert Earthquake Early Warning System. *Bulletin of the Seismological Society of America*, 113(3): 1286–1310, 02 2023. doi: [10.1785/0120220181](https://doi.org/10.1785/0120220181).
- Nuyen, C. P. and Schmidt, D. A. Filling the Gap in Cascadia: The

- Emergence of Low-Amplitude Long-Term Slow Slip. *Geochemistry, Geophysics, Geosystems*, 22(3):e2020GC009477, 2021. doi: <https://doi.org/10.1029/2020GC009477>.
- Okada, Y. Surface deformation due to shear and tensile faults in a half-space. *Bulletin of the seismological society of America*, 75(4):1135–1154, 1985. doi: <https://doi.org/10.1785/BSSA0750041135>.
- Peters, R., Jaffe, B., and Gelfenbaum, G. Distribution and sedimentary characteristics of tsunami deposits along the Cascadia margin of western North America. *Sedimentary Geology*, 200(3):372–386, 2007. doi: <https://doi.org/10.1016/j.sed-geo.2007.01.015>.
- Satake, K., Wang, K., and Atwater, B. F. Fault slip and seismic moment of the 1700 Cascadia earthquake inferred from Japanese tsunami descriptions. *Journal of Geophysical Research: Solid Earth*, 108(B11), 2003. doi: <https://doi.org/10.1029/2003JB002521>.
- Synolakis, C. E., Bernard, E. N., Titov, V. V., Kânoğlu, U., and González, F. I. *Validation and Verification of Tsunami Numerical Models*, pages 2197–2228. Birkhäuser Basel, Basel, 2009. doi: [10.1007/978-3-0346-0057-6_11](https://doi.org/10.1007/978-3-0346-0057-6_11).
- Tang, L., Titov, V. V., and Chamberlin, C. D. Development, testing, and applications of site-specific tsunami inundation models for real-time forecasting. *Journal of Geophysical Research: Oceans*, 114(C12), 2009. doi: <https://doi.org/10.1029/2009JC005476>.
- Titov, V., Kânoğlu, U., and Synolakis, C. Development of MOST for Real-Time Tsunami Forecasting. *Journal of Waterway, Port, Coastal, and Ocean Engineering*, 142(6):03116004, 2016. doi: [10.1061/\(ASCE\)WW.1943-5460.0000357](https://doi.org/10.1061/(ASCE)WW.1943-5460.0000357).
- Wei, Y., Bernard, E. N., Tang, L., Weiss, R., Titov, V. V., Moore, C., Spillane, M., Hopkins, M., and Kânoğlu, U. Real-time experimental forecast of the Peruvian tsunami of August 2007 for U.S. coastlines. *Geophysical Research Letters*, 35(4), 2008. doi: <https://doi.org/10.1029/2007GL032250>.
- Williamson, A. L., Melgar, D., Crowell, B. W., Arcas, D., Melbourne, T. I., Wei, Y., and Kwong, K. Toward Near-Field Tsunami Forecasting Along the Cascadia Subduction Zone Using Rapid GNSS Source Models. *Journal of Geophysical Research: Solid Earth*, 125(8):e2020JB019636, 2020. doi: <https://doi.org/10.1029/2020JB019636>.
- Wright, T. J., Houlié, N., Hildyard, M., and Iwabuchi, T. Real-time, reliable magnitudes for large earthquakes from 1 Hz GPS precise point positioning: The 2011 Tohoku-Oki (Japan) earthquake. *Geophysical Research Letters*, 39(12), 2012. doi: <https://doi.org/10.1029/2012GL051894>.

The article *Performance of Slab Geometry Constraints on Rapid Geodetic Slip Models, Tsunami Amplitude, and Inundation Estimates in Cascadia* © 2025 by Kevin Kwong is licensed under CC BY 4.0.